Neuropharmacology 143 (2018) 122–129

Contents lists available at ScienceDirect

Neuropharmacology

journal homepage: www.elsevier.com/locate/neuropharm

Incomplete block of NMDA receptors by intracellular MK-801

Weinan Sun[a,1], Jonathan M. Wong[b,c], John A. Gray[b,d,**], Brett C. Carter[a,e,*]

[a] Vollum Institute, Oregon Health & Science University, Portland, USA
[b] Center for Neuroscience, University of California, Davis, USA
[c] Neuroscience Graduate Program, University of California, Davis, USA
[d] Neurology Department, University of California, Davis, USA
[e] European Neuroscience Institute Göttingen, Germany

HIGHLIGHTS

- Intracellular MK-801 does not completely block synaptic NMDAR current.
- Heterologously expressed NMDARs also show incomplete inhibition by iMK-801.
- Modeling indicates a ~30,000 fold lower affinity for intracellular MK-801.

ABSTRACT

NMDA receptors (NMDARs) are essential components in glutamatergic synaptic signaling. The NMDAR antagonist MK-801 has been a valuable pharmacological tool in evaluating NMDAR function because it binds with high affinity to the NMDAR ion channel pore and is non-competitive with ligand binding. MK-801 has also been used to selectively inhibit NMDAR current in only the cell being recorded by including the drug in the intracellular recording solution. Here, we report that intracellular MK-801 (iMK-801) only partially inhibits synaptic NMDAR currents at +40 mV at both cortical layer 4 to layer 2/3 and hippocampal Schaffer collateral to CA1 synapses. Furthermore, iMK-801 incompletely inhibits heterologously expressed NMDAR currents at −60 mV, consistent with a model of iMK-801 having a very slow binding rate and consequently ~30,000 times lower affinity than MK-801 applied to the extracellular side of the receptor. While iMK-801 can be used as a qualitative tool to study reduced postsynaptic NMDAR function, it cannot be assumed to completely block NMDARs at concentrations typically used in experiments.

1. Introduction

NMDARs are ion channels that open in response to binding of the agonist glutamate and co-agonist glycine (or D-serine; Johnson and Ascher, 1987; Kleckner and Dingledine, 1988) in addition to coincident depolarization that relieves Mg^{2+} block of the ion channel pore (Mayer et al., 1984; Nowak et al., 1984). NMDAR current contributes to synaptic depolarization and has a large Ca^{2+} conductance (MacDermott et al., 1986; Jahr and Stevens, 1993; Burnashev et al., 1995) which is involved in initiating intracellular signaling events, including synaptic plasticity (Lynch et al., 1983; Luscher and Malenka, 2012). Many pharmacological tools have been developed to manipulate NMDAR function (Traynelis et al., 2010).

The NMDAR antagonist MK-801 has been particularly useful in studying fundamental properties of glutamatergic synapses. MK-801 binds with high affinity when applied extracellularly (~5–30 nM dissociation constant at −70 mV; Dravid et al., 2007) to the NMDAR ion channel pore only when the receptor is active and prevents ionic current through the channel (Huettner and Bean, 1988). The combination of state-dependence and high-affinity binding has made possible the measurement of several facets of glutamatergic synaptic signaling. For example: MK-801 has been used to measure the biophysical property of ion channel open probability in response to glutamate (Jahr, 1992), the probability of vesicle release from the presynaptic terminal (Rosenmund et al., 1993), and the motility of NMDARs in the postsynaptic membrane (Tovar and Westbrook, 2002). MK-801 has also been used to selectively inhibit NMDARs in single cells by introducing the drug into the intracellular environment through a recording pipette (Berretta and Jones, 1996). Because intracellular MK-801 (iMK-801) can only access NMDAR in the selected cell, it has been used to investigate the NMDAR contribution to synaptic signaling and integration independent of possible network effects of blocking NMDARs globally

* Corresponding author. University Medical Center Goettingen in cooperation with Max-Planck-Society, European Neuroscience Institute, Grisebachstrasse 5, D-37077 Goettingen, Germany.
** Corresponding author. Center for Neuroscience, University of California, Davis, 1544 Newton Court, Davis, CA 95618, USA.
E-mail addresses: john.gray@ucdavis.edu (J.A. Gray), b.carter@eni-g.de (B.C. Carter).
[1] Present address: Howard Hughes Medical Institute, Janelia Research Campus, Ashburn, VA, USA.

https://doi.org/10.1016/j.neuropharm.2018.09.022
Received 5 September 2018; Received in revised form 12 September 2018; Accepted 12 September 2018
Available online 15 September 2018
0028-3908/

(e.g. Lavzin et al., 2012; Smith et al., 2013). This manipulation has also led to the suggestion that, at some synapses, NMDARs may be functioning presynaptically (Berretta and Jones, 1996; Humeau et al., 2003; Sjöstrom et al., 2003; Bender et al., 2006; Nevian and Sakmann, 2006; Corlew et al., 2007; Rodriguez-Moreno et al., 2011; Bouvier et al., 2015), or postsynaptically in a manner independent of ion flux through the NMDAR (Carter and Jahr, 2016). However, many of these interpretations of iMK-801 effects rely on the assumption that iMK-801 blocks NMDARs completely.

In this study, we tested whether iMK-801 was effective in inhibiting NMDAR currents. At the synapse between cortical layer 4 (L4) to layer 2/3 (L2/3) in rat somatosensory cortex, the commonly used concentration of iMK-801, 1 mM, reduced, but did not eliminate NMDAR currents. Similarly, at the hippocampal Schaffer collateral to CA1 neuron synapse, iMK-801 reduced, but did not eliminate NMDAR currents. We then tested iMK-801 in heterologously expressed NMDARs and found a reduction of NMDAR current, but the inhibition was incomplete. These results were recapitulated in a NMDAR kinetic model in which the rate of iMK-801 binding was ~30,000 times slower than extracellularly applied MK-801. These results show that iMK-801 can be used to qualitatively reduce NMDAR currents, but complete inhibition cannot be assumed.

2. Materials and methods

2.1. Cortical slice preparation and electrophysiology

Young (postnatal day 13–21) Sprague-Dawley rats (Charles River) of either sex were anesthetized with isoflurane and decapitated. The brain was removed into warm ACSF consisting of (in mM): 119 NaCl, 2.5 KCl, 25 $NaHCO_3$, 1.25 NaH_2PO_4, 2 $CaCl_2$, 1 $MgCl_2$, 10 Glucose, 1.3 sodium Ascorbate, 3 sodium pyruvate, equilibrated with 95% O_2/5% CO_2 (chemicals from Sigma). The brain was blocked at 35° from the coronal plane (Agmon and Connors, 1991), and 300 μm slices containing Barrel Cortex were cut with a vibratome (Leica VT1200S) in 37 °C ACSF. Slices recovered in 37 °C ACSF for 30 min and were maintained at room temperature (~22 °C) until use. Animal handling and procedures followed OHSU IACUC approved protocols.

Slices were transferred to a recording chamber perfused with 35 °C ACSF at a rate of ~2 mL/min. Barrel cortex was visually identified and two theta glass stimulation pipettes filled with ACSF were placed in layer 4 and used to stimulate two independent synaptic pathways. L2/3 pyramidal neurons in the same column were then visually identified and patched with borosilicate glass pipettes (2–4 MΩ) filled with an internal solution consisting of (in mM): 108 cesium methanesulfonate or cesium gluconate, 2.8 NaCl, 20 HEPES, 0.4 EGTA, 5 tetraethylammonium chloride, pH adjusted to 7.3 with CsOH. (+)-MK-801 (Tocris) was added to the internal solution from a 100 mM (in water) stock solution. After break-in, the L2/3 neuron was voltage-clamped at −70 mV and L4 was stimulated at 0.1 Hz and inward currents were measured. Picrotoxin (50 μM, Sigma) and NBQX (5 μM, Tocris) were then applied to block $GABA_A$ and AMPA receptors, respectively. The cell was then held at +40 mV to relieve Mg^{2+} block and measure outward NMDAR currents, followed by bath application of 10 μM R-CPP (Tocris) to block NMDAR currents. Peak inward and outward currents were measured from averaged traces in each condition. Data were acquired using a Multiclamp 700B (Molecular devices), controlled by Scanimage software (Pologruto et al., 2003), sampled at 10 kHz, and analyzed using Igorpro (Wavemetrics). Series resistance was monitored and not compensated. Junction potential corrections were not made.

2.2. Hippocampal slice preparation and electrophysiology

All mice were of C57BL/6J background and housed according to IACUC guidelines at the University of California Davis. P18-24 mice were anesthetized in isoflurane, and decapitated. Brains were rapidly removed and placed in ice-cold sucrose cutting buffer, containing (in mM) 210 sucrose, 25 $NaHCO_3$, 2.5 KCl, 1.25 NaH_2PO_4, 7 glucose, 7 $MgCl_2$, 0.5 $CaCl_2$. Transverse 300 μm hippocampal slices were cut on a Leica VT1200 vibratome (Buffalo Grove, IL) in ice-cold cutting buffer. Slices were recovered in 32 °C artificial cerebrospinal fluid (ACSF) solution, containing (in mM) 119 NaCl, 26.2 $NaHCO_3$, 11 glucose, 2.5 KCl, 1 NaH_2PO_4, 2.5 $CaCl_2$ and 1.3 $MgSO_4$, for 1 h before recording. Slices were transferred to a submersion chamber on an upright Olympus microscope, perfused in room temperature normal ACSF containing picrotoxin (0.1 mM) and saturated with 95% O_2/5% CO_2. CA1 neurons were visualized by infrared differential interference contrast microscopy. Cells were patched with 3–5 MΩ borosilicate pipettes filled with intracellular solution, containing (in mM) 135 cesium methanesulfonate, 8 NaCl, 10 HEPES, 0.3 Na-GTP, 4 Mg-ATP, 0.3 EGTA, and 5 QX-314 (Sigma, St Louis, MO). (+)-MK-801 (Abcam) was added to the internal solution from a 100 mM (in DMSO) stock solution to a final concentration of 1 mM and 1% DMSO. Control experiments with simultaneous whole cell recordings with internal solutions containing 1% DMSO and 0% DMSO showed no difference in NMDAR-EPSCs (data not shown). Excitatory postsynaptic currents (EPSCs) were evoked by electrical stimulation of Schaffer collaterals with a bipolar electrode (MicroProbes, Gaithersburg, MD). AMPAR-EPSCs were measured at a holding potential of −70 mV, and NMDAR-EPSCs were measured at +40 mV in the presence of 10 μM NBQX. During paired-pulse stimulation, only the response to the first stimulation was measured and reported. Series resistance was monitored and not compensated, and cells were discarded if series resistance varied more than 25%. All recordings were obtained with a Multiclamp 700B amplifier (Molecular Devices, Sunnyvale, CA), filtered at 2 kHz, digitized at 10 kHz. Analysis was performed with the Clampex software suite (Molecular Devices, Sunnyvale, CA) and Prism 7 software (GraphPad). Junction potential corrections were not made.

2.3. Recombinant expression and recording

HEK293 cells were transfected with plasmid cDNAs encoding Rat GluN1-1a (GenBank: U08261) and GluN2A (GenBank D13211) subunits at a ratio of 1:2 using the calcium phosphate precipitation method as previously described (Hansen et al., 2014). Whole-cell voltage-clamp recordings were performed using an Axopatch 1D amplifier (Molecular Devices, Union City, CA) at room temperature. The holding potential was −60 mV. The electrodes were filled with internal solution containing (in mM) 110 D-gluconate, 110 CsOH, 30 CsCl, 5 HEPES, 4 NaCl, 0.5 $CaCl_2$, 2 $MgCl_2$, 5 BAPTA, 2 Na-ATP, and 0.3 Na-GTP (pH 7.35 with CsOH), and the extracellular recording solution was composed of (in mM) 150 NaCl, 10 HEPES, 3 KCl, 0.5 $CaCl_2$, 0.1 Glycine, 0.01 EDTA, 20 D-mannitol (pH 7.4 with NaOH). (+)-MK-801 (Tocris) was added to the internal solution from a 100 mM (in water) stock solution. Rapid solution exchange (open tip solution exchange had 10–90% rise times below 1 msec) was achieved using a two-barrel theta-glass pipette controlled by a piezobimorph. Data were acquired at 20 kHz, filtered at 5–10 kHz, and analyzed with Axograph software (axograph.com) and IgorPro (Wavemetrics). Junction potential and series resistance corrections were not made.

2.4. Statistical analysis

Values are reported as the mean ± SEM. At least two animals were used per group. Comparisons were made using paired or unpaired *t*-test where appropriate. Statistical significance is reported if $p < 0.05$. Experiments were not performed blind to the condition of the experiments. Sample sizes are similar to those generally used in the field, and no statistical methods were used to predetermine the sample size. Randomization was not used to determine experimental conditions.

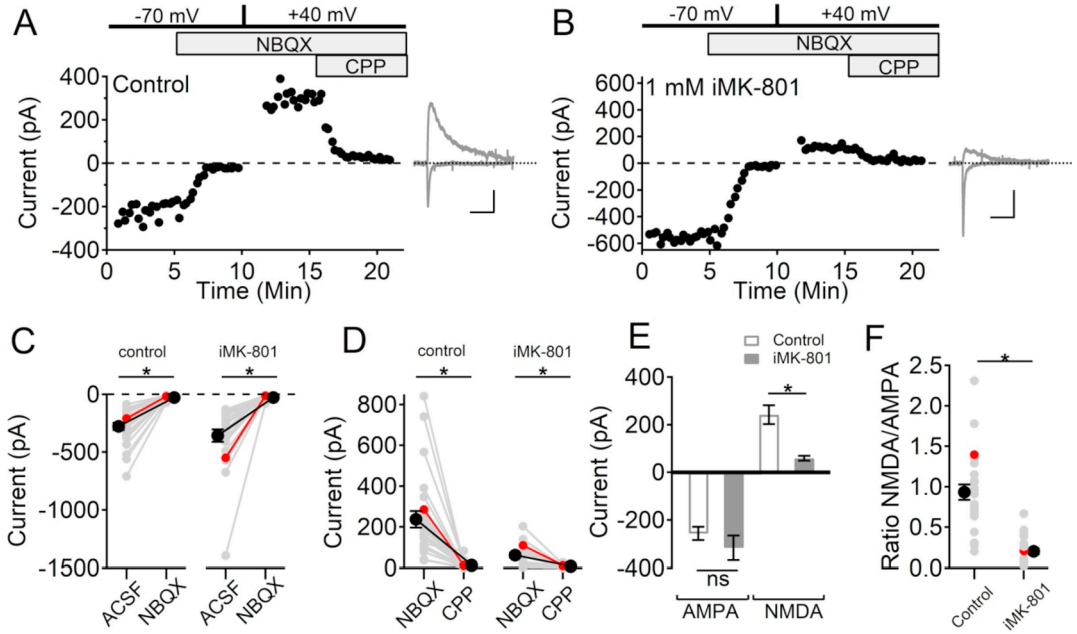

Fig. 1. Intracellular MK-801 inhibits synaptic NMDAR current, but not completely. (A) Example recording of synaptic AMPAR and NMDAR currents from a L2/3 neuron while stimulating L4 at 0.1 Hz. Left: time course of peak synaptic currents, measuring inward currents while holding the postsynaptic neuron at −70 mV, and outward currents at +40 mV. 5 μM NBQX was added to block AMPAR currents and 10 μM CPP was added to block NMDAR currents. Right: AMPAR (downward current) and NMDAR current (upward currents) isolated by subtraction of traces before and after antagonist addition. Scale bars are 100 ms, 100 pA. (B) Example time course (left) and traces (right) from a recording with 1 mM MK-801 included in the internal solution. Scale bars are 100 ms, 200 pA. (C) Summary of inward currents measured at −70 mV before (ACSF) and after 5 μM NBQX addition using control internal solution (left, N = 25 synaptic pathways from 13 neurons, $t_{(24)}$ = 9.07, p = 3.2e-9, paired *t*-test), and with 1 mM iMK-801 (right, N = 24 synaptic pathways from 13 neurons, $t_{(23)}$ = 6.32, p = 1.9e-6, paired *t*-test). (D) Summary of outward currents measured at +40 mV before and after 10 μM R-CPP addition using control internal solution (left, N = 25 synaptic pathways from 13 neurons, $t_{(24)}$ = 5.82, p = 5.4e-6, paired *t*-test), and with 1 mM iMK-801 (right, N = 24 pathways from 13 neurons, $t_{(23)=5.07}$, p = 3.9e-5, paired *t*-test). (E) Summary of AMPAR currents isolated by NBQX subtraction (ns, not significant, $t_{(47)}$ = 1.34, p = 0.19, *t*-test) and NMDAR currents isolated by R-CPP subtraction ($t_{(47)}$ = 4.38, p = 6.7e-5, *t*-test) with or without MK-801 in the recording pipette. (F) The ratio of NMDAR to AMPAR currents was reduced in the iMK-801 condition (right) compared to control internal solution (left, $t_{(47)}$ = 7.27, p = 3.2e-9, *t*-test). Red symbols in (C), (D), and (F) are data from the examples shown in (A) and (B). The * symbol indicates p < 0.05. (For interpretation of the references to colour in this figure legend, the reader is referred to the web version of this article.)

3. Results

3.1. Synaptic NMDAR currents are reduced, but not eliminated by 1 mM iMK-801

To test the effect of iMK-801 on synaptic NMDARs, we recorded synaptic currents from L2/3 neurons in rat somatosensory cortical slices in response to L4 stimulation. Fig. 1A shows an example recording using control internal solution (without added MK-801). After breaking into the L2/3 neuron, voltage-clamp was established and the neuron was held at −70 mV while L4 was stimulated at 0.1 Hz. NBQX (5 μM) and picrotoxin (50 μM) were then added to block AMPA and $GABA_A$ receptors, respectively. The neuron was then held at +40 mV to relieve Mg^{2+} block, outward currents were measured, and the NMDAR antagonist R-CPP (10 μM) was added. AMPAR and NMDAR currents were then isolated by subtraction of traces obtained in the presence of the specific antagonists (Fig. 1A, inset). In the example shown in Fig. 1A, the peak AMPAR current was −198 pA and the peak NMDAR current was 276 pA, giving a ratio of NMDAR/AMPAR current of 1.39. Fig. 1B shows a similar experiment except the internal recording solution contained 1 mM MK-801. Inward currents measured at −70 mV were blocked by NBQX, and outward currents measured at +40 mV were blocked by R-CPP. In this example recording, the peak AMPAR current was −542 pA and the peak NMDAR current was 111 pA, giving a ratio of 0.20. NBQX decreased inward currents using either control internal solution (Fig. 1C, −277.5 ± 30.4 pA to −28.1 ± 3.5 pA, N = 25 synaptic pathways from 13 neurons, $t_{(24)}$ = 9.07, p = 3.2e-9, paired *t*-test), or internal solution containing 1 mM MK-801 (from −357.0 ± 54.1 pA to −28.4 ± 3.5 pA, N = 24 synaptic pathways from 13 neurons, $t_{(23)}$ = 6.32, p = 1.9e-6, paired *t*-test). R-CPP reduced outward currents in experiments using control internal solution (Fig. 1D, from 246.0 ± 40.2 pA to 13.5 ± 3.4 pA, N = 25, $t_{(24)}$ = 5.82, p = 5.4e-6, paired *t*-test), as well as in experiments using 1 mM iMK-801 containing internal solution (Fig. 1D, from 61.3 ± 10.8 pA to 8.5 ± 1.4 pA, N = 24, $t_{(23)}$ = 5.07, p = 3.9e-5, paired *t*-test). Fig. 1E shows a summary of the AMPAR and NMDAR currents isolated by antagonist subtraction. There was no significant difference between the AMPAR current level measured using either control or 1 mM iMK-801 internal solution (control internal: −256.9 ± 27.9 pA, N = 25, iMK-801: −335.8 ± 51.8 pA, N = 24, $t_{(47)}$ = 1.34, p = 0.19, *t*-test). 1 mM iMK-801 significantly inhibited the NMDAR current to ~25% of the control level (control: 241.4 ± 39.7 pA, N = 25, iMK-801: 61.5 ± 10.6 pA, N = 24, $t_{(47)}$ = 4.38, p = 6.7e-5, *t*-test). In addition, the synaptic NMDAR/AMPAR ratio was significantly reduced in the iMK-801 condition relative to control (Fig. 1F, control NMDAR/AMPAR ratio: 0.93 ± 0.09, N = 25, iMK-801 ratio: 0.20 ± 0.03, N = 24, $t_{(47)}$ = 7.27, p = 3.2e-9).

3.2. Incomplete block of NMDAR currents by intracellular MK-801 in hippocampal CA1 neurons

In addition to L4-to-L2/3 synapses, the efficacy of iMK-801 at blocking synaptic NMDAR currents was also examined at the prototypical CA3-to-CA1 synapse. As a control, extracellular MK-801 (50 μM) was shown to effectively block synaptic NMDAR currents within 15 min of repeated stimulation of the Schaffer collateral axons (Fig. 2A). To increase the probability of synaptic vesicle release at individual synapses without inducing postsynaptic plasticity, a paired-pulse

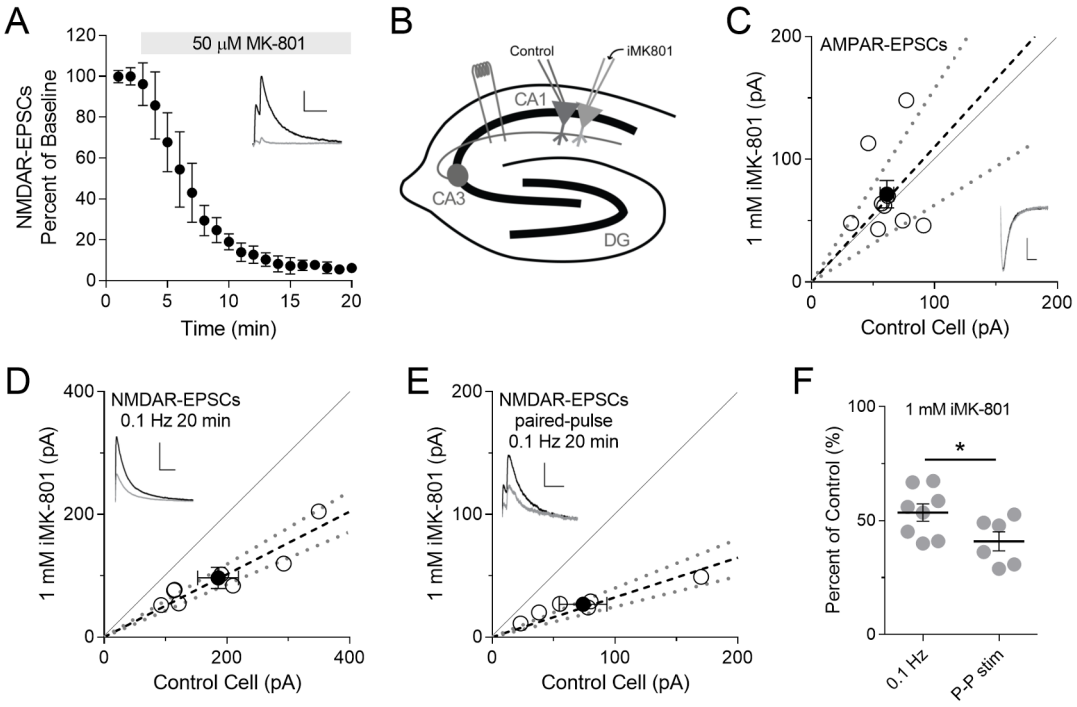

Fig. 2. Incomplete block of synaptic NMDAR currents by intracellular MK-801 at the Schaffer collateral to CA1 synapse. (A) Complete block of evoked NMDAR-EPSC amplitudes in 50 μM extracellular MK-801 measured at +40 mV. Baseline NMDAR-EPSC amplitudes were obtained for 2 min then a paired-pulse stimulation protocol (two pulses 50 msec apart repeated at 0.1 Hz) was applied. Data represent the mean ± SEM of the first NMDAR-EPSC amplitude normalized to the average baseline amplitude (n = 7). Inset, sample traces of NMDAR-EPSCs at baseline (black) and after paired-pulse stimulation (gray) in 50 μM MK-801; scale bars represent 100 pA, 200 msec. (B) Schematic of simultaneous whole-cell recordings from neighboring CA1 neurons, one with control solution, and the other with internal containing 1 mM iMK-801. (C) AMPAR-EPSCs are unchanged by 1 mM iMK-801. Scatterplot of AMPAR-EPSC amplitudes measured at −70 mV from individual neuron pairs (open circles) and averaged pair ± SEM (solid circle) (control: 61.3 ± 5.8 pA, iMK-801: 71.6 ± 11.0 pA; n = 9, $t_{(8)}$ = 0.8023, p = 0.446, paired *t*-test). Dashed lines represent linear regression and 95% confidence interval. Inset, sample traces of AMPAR-EPSCs (black, control; gray iMK-801); scale bars represent 20 pA, 20 msec. (D–F) Incomplete block of NMDAR-EPSCs by iMK-801. Amplitudes were measured after 20 min of either 0.1 Hz stimulation while holding at +40 mV (D) or 20 min of a paired-pulse stimulation protocol (E, two pulses at a 50 msec interval repeated at 0.1 Hz). Scatterplots represent NMDAR-EPSC amplitudes from individual neuron pairs (open circles) and mean ± SEM (solid circle). Insets, sample traces of NMDAR-EPSCs (black, control; gray iMK-801); scale bars represent 100 pA, 200 msec. (F) Paired-pulse stimulation lead to significantly more, yet still incomplete, NMDAR inhibition by iMK-801 (0.1Hz for 20 min: 53.6 ± 3.8% of control, n = 8; paired pulse: 40.9 ± 4.2% of control, n = 6; $t_{(12)}$ = 2.223, p = 0.046, *t*-test).

stimulation protocol (two pulses 50 msec apart repeated at 0.1 Hz) was utilized. To examine the efficacy of iMK-801, we performed simultaneous whole cell recordings from neighboring CA1 pyramidal neurons with either control internal solution or internal solution containing 1 mM iMK-801 (Fig. 2B). Simultaneous paired whole-cell recordings at CA3-to-CA1 synapses provide a rigorous, quantitative, and internally controlled comparison of the effects of iMK-801. At the commonly used concentration of 1 mM, iMK-801 may have off-target effects; however, no effects were observed on AMPAR-EPSCs (Fig. 2C; control: 61.3 ± 5.8 pA, iMK-801: 71.6 ± 11.0 pA; n = 9, $t_{(8)}$ = 0.8023, p = 0.446, paired *t*-test). NMDAR-EPSCs were then examined at +40 mV in the presence of 10 μM NBQX to block AMPARs. After 20 min of simulating Schaffer collaterals at a neutral rate of 0.1 Hz, iMK-801 inhibited the synaptic NMDAR currents to ~50% of control levels (Fig. 2D; control: 185.7 ± 33.2 pA, iMK-801: 96.4 ± 17.4 pA; n = 8, $t_{(7)}$ = 4.782, p = 0.0020, paired *t*-test). Increasing synaptic release probability by using a paired-pulse protocol (2 pulses at 50 msec interval, repeated at 0.1 Hz) led to increased NMDAR current inhibition by iMK-801 to ~40% of control levels (Fig. 2E; control: 74.0 ± 21.2 pA, iMK-801: 26.7 ± 5.2 pA; n = 6, $t_{(5)}$ = 2.904, p = 0.0336, paired *t*-test). Thus, while increased stimulation led to a modest increase in synaptic NMDAR current inhibition (Fig. 2F; current in the presence of iMK-801 relative to control measured after 0.1 Hz stimulation for 20 min: 53.6 ± 3.8%, n = 8; after paired pulse stimulation: 40.9 ± 4.2%, n = 6; $t_{(12)}$ = 2.223, p = 0.046, *t*-test), the block was still incomplete.

3.3. Recombinant NMDARs are inhibited, but not completely blocked by 1 mM intracellular MK-801

The recordings of synaptic currents shown in Figs. 1 and 2 were obtained from intact neurons in brain slices that have processes extending for hundreds of micrometers, and the exact location of the stimulated synapses was not known. In addition, voltage clamp of synapses on dendritic spines in intact neurons is not well experimentally controlled (Beaulieu-Laroche and Harnett, 2018). While the inhibition of NMDAR currents by iMK-801 indicates that the drug reached and interacted with the synaptic receptors, the concentration of MK-801 at the synapse was not known with certainty. Therefore, we tested the effects of 1 mM iMK-801 on NMDAR currents in a heterologous expression system (Fig. 3). The NMDAR GluN1 and GluN2A subunits were expressed in HEK293 cells and whole cell voltage clamp recordings were then made from isolated cells. In these experiments, Mg^{2+} was excluded from the extracellular solution, which contained 100 μM glycine, and L-glutamate (1 mM) was delivered by a fast-flow exchange system to activate the NMDARs. Fig. 3A shows a recording using the control internal solution while voltage-clamping the cell at −60 mV. In this example recording, the NMDAR current reached a peak of −839 pA which was followed by a desensitization to a steady-state level 63% of the peak current level. In 7 cells using control internal solution, the peak NMDAR current induced by 1 mM glutamate was −1.92 ± 0.77 nA. On average, the steady-state NMDAR current level was 55 ± 6% of the peak current and developed over a time course that could be fit with a single exponential with a time constant of

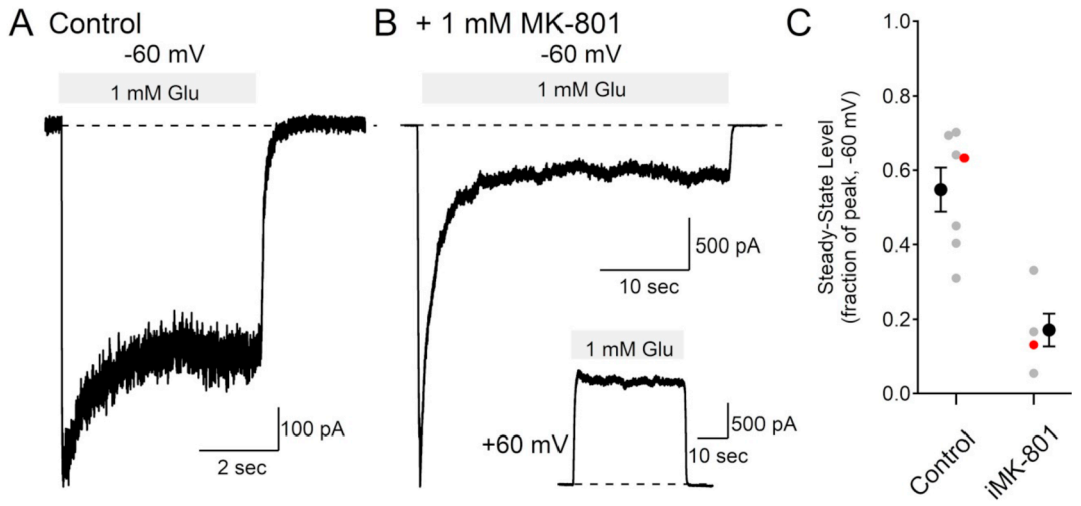

Fig. 3. Incomplete inhibition of NMDAR currents by intracellular MK-801 in HEK293 cells expressing GluN1/GluN2A recombinant receptors. (A) Using control internal solution and holding at −60 mV, 1 mM L-Glutamate induced an inward current that desensitized to 63% of the peak level. (B) With 1 mM MK-801 in the intracellular solution, glutamate induced current fell to 13% of the peak value (note the different time scale from panel (A)). The inset shows a recording from the same cell held at +60 mV. (C) Summary of steady-state current as a fraction of the peak current at −60 mV in 7 cells using control internal solution (0.55 ± 0.06, mean ± SEM) and in 4 cells with 1 mM intracellular MK-801 (0.17 ± 0.04, mean ± SEM, $t_{(9)}$ = 4.56, p = 1.4e-3, *t*-test). The red markers are from the example traces in (A) and (B). (For interpretation of the references to colour in this figure legend, the reader is referred to the web version of this article.)

1.06 ± 0.23 s. Fig. 3B shows an example recording of NMDAR currents with 1 mM MK-801 in the recording pipette. In this example holding at −60 mV, after reaching a peak inward current of −3.45 nA, the current decayed to a steady-state level 13% of the peak level. In 4 cells recorded with 1 mM iMK-801, the mean peak inward current was −2.59 ± 0.53 nA, not significantly different from the control recordings ($t_{(9)}$ = 0.71, p = 0.50, *t*-test). The steady-state current level with 1 mM iMK-801 was on average 17 ± 4% of the peak current, corresponding to an inhibition of NMDAR currents by iMK-801 to ~31% of the control steady-state current level (Fig. 3C, $t_{(9)}$ = 4.56, p = 1.9e-3, *t*-test). The time course of decay of current in the presence of 1 mM iMK-801 could be fit with a double exponential function in which the fast component was set to the average time constant of desensitization measured in the control condition (1.06 s), and the second, slower component was 4.95 ± 1.87 s.

At positive voltages, extracellular MK-801 dissociates from the NMDAR more readily than at negative voltages (Huettner and Bean, 1988). Similarly, inhibition of NMDAR current by intracellular MK-801 showed voltage dependence (Fig. 3B). At +60 mV, NMDAR currents in cells filled with 1 mM iMK-801 reached a steady-state level 85 ± 5% of the peak current level (mean ± SEM, N = 4), significantly larger than the steady-state current from the same cells measured at −60 mV ($t_{(3)}$ = 8.9, p = 1.2e-4, paired *t*-test).

3.4. An NMDAR model can recapitulate the intracellular MK-801 block

Fig. 4A shows a Markov model structure for NMDAR glutamate binding and gating based on the model of Lester and Jahr (1992). Following the binding of two glutamate molecules to the receptor, the channel can either open or enter a desensitized state. If MK-801 is present, the drug has access only to the open channel state, and when MK-801 is bound, the receptor can gate normally, but does not conduct current. The rate constants of glutamate binding and unbinding were initially set similar to recombinant GluN1/2A receptors (Maki and Popescu, 2014). Peak open probability in the model is ~0.46, similar to that measured from GluN1/2A receptors (Erregar et al., 2005), and, in the absence of MK-801, the conductance desensitizes to a steady-state level that is ~60% of the peak, similar to the value measured in the recombinant receptors (Fig. 3C). The rate constant of MK-801 unbinding was estimated from the rate of recovery from MK-801 block measured in dissociated neurons. The rate of recovery is a product of the open probability, p_{open}, and the voltage dependent dissociation constant (Huettner and Bean, 1988). Fitting the measured recovery time constants (from Huettner and Bean, 1988: 92 ± 40 min at −70 mV and 1.8 ± 0.3 min at +30 mV, and estimated p_{open} in those recordings ranged from 0.002 to 0.007) to an exponential function of voltage (p_{open} *k_0*exp (V/k_1), gave the voltage dependent function 0.00285* exp (V_m/25.4) s^{-1}. The on-rate of MK-801 was then adjusted to empirically match the time course of block measured in recombinant receptors (Fig. 3B). This led to an estimated on-rate of 8e-4 $\mu M^{-1}s^{-1}$, which captures well the time course and degree of inhibition by 1 mM intracellular MK-801 on the NMDAR conductance (Fig. 4C). In the absence of MK-801, the modeled conductance desensitizes to a level similar to the measured levels (Fig. 4B, dashed trace). When 1 mM MK-801 is included in the model, the conductance (Fig. 4C, solid red trace) matches very closely the measured NMDAR conductance time course (Fig. 4C, black trace, same trace as in Fig. 3B). These modeled rates correspond to an affinity of MK-801 to the NMDAR that is ~30,000 times lower when applied to the intracellular side of the receptor than when applied extracellularly.

4. Discussion

4.1. The binding site of MK-801

The binding site of intracellularly applied MK-801 was presumed to be the same site as extracellularly applied MK-801. Consistent with this interpretation, iMK-801 required opening of the channel to inhibit NMDAR current: in recombinant receptors, the current reaches a peak before being inhibited to a lower steady-state level and the peak current was similar in amplitude in both control and iMK-801 conditions (Fig. 3). The inhibition by iMK-801 shows voltage dependence consistent with the expulsion of positively charged MK-801 across the membrane through the ion channel. A single binding site for iMK-801 is also consistent with recent cryo-EM structural data (Lu et al., 2017) and x-ray crystallographic data (Song et al., 2018) that show a single MK-801 binding site in the NMDAR channel.

The voltage-dependent off-rate of MK-801 in the model matches the measured rates of recovery in isolated neuronal cells (Huettner and Bean, 1988). This similarity in measured and modeled MK-801 off-rate

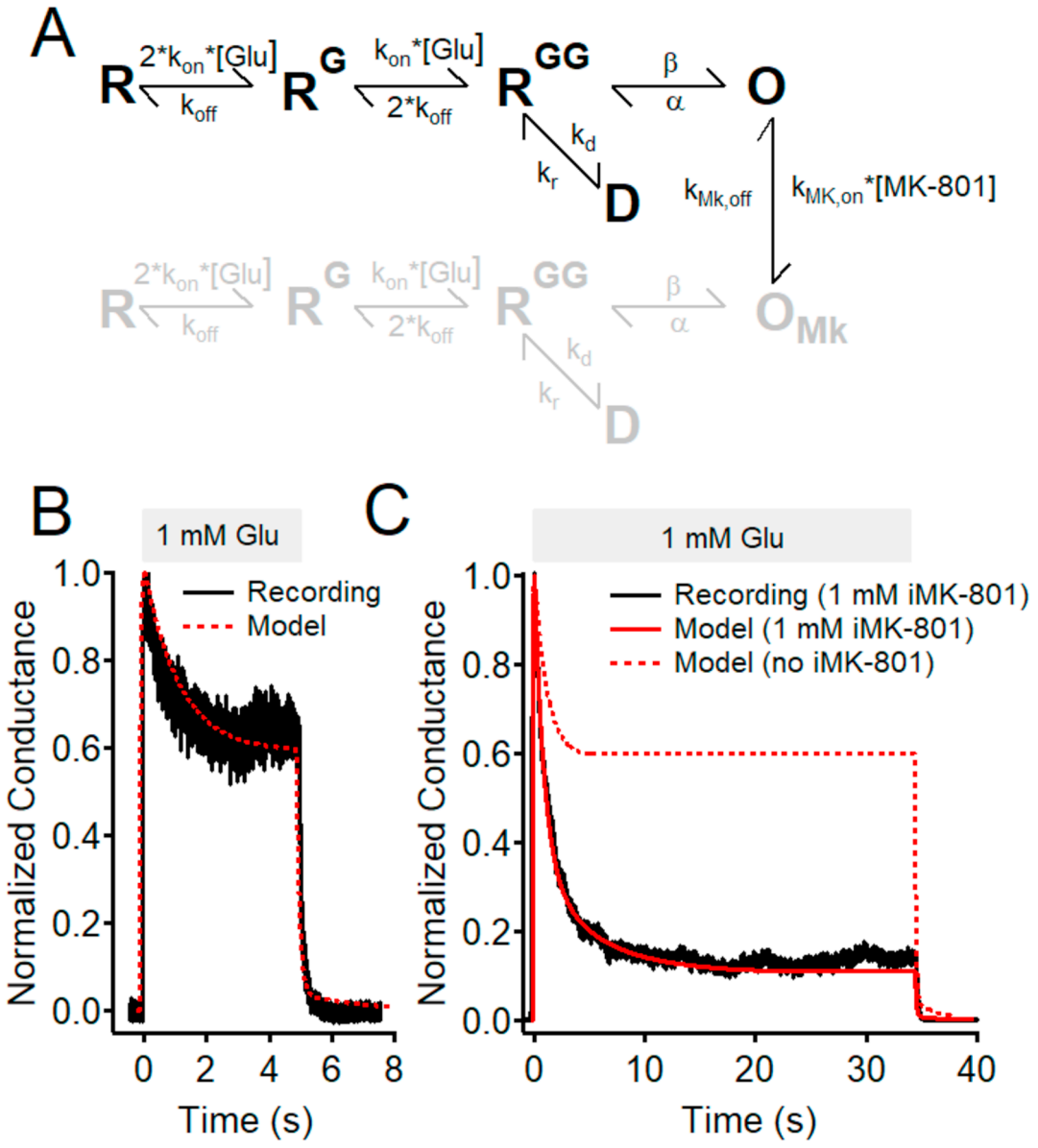

Fig. 4. A NMDAR model can recapitulate inhibition by iMK-801. (A) Structure of the NMDAR model consisting of the unliganded receptor, R, two binding sites for glutamate, R^G and R^{GG}, a desensitized state D, open state O, and corresponding states with MK-801 bound (shown in gray). After two glutamate molecules bind to the receptor, the channel can open or desensitize (black states). MK-801 has access to the channel only during the open state. Once bound, the channel does not conduct current, but can gate normally (gray states). (B) Normalized modeled NMDAR conductance at −60 mV (dashed red trace) matches well the recorded NMDAR conductance (black trace, same recording as Fig. 3A). (C) Modeling NMDAR conductance at −60 mV with 1 mM iMK-801 (solid red trace) matches well the time course of the recorded NMDAR conductance (black trace, same recording as Fig. 3B). The red dashed trace shows the modeled current in the absence of iMK-801. The model rates used were: k_{on} = 20 $\mu M^{-1}s^{-1}$, k_{off} = 60 s^{-1}, k_d = 6.5 s^{-1}, k_r = 0.5 s^{-1}, α = 250 s^{-1}, β = 2000 s^{-1}, $k_{Mk,on}$ = 8e-4 $\mu M^{-1}s^{-1}$, $k_{Mk,off}$ = 0.179 s^{-1}. (For interpretation of the references to colour in this figure legend, the reader is referred to the web version of this article.)

is consistent with MK-801 binding at the same site—whether MK-801 enters from the extra- or intracellular side of the receptor, the unbinding rate is equivalent. The primary difference between intra- and extracellularly applied MK-801 was found to be the on-rate of the drug. The modeled on-rate, $8 \times 10^{-4}\,\mu M^{-1}s^{-1}$, ~30,000 times slower than the measured on-rate of extracellularly applied MK-801, $23.7\,\mu M^{-1}s^{-1}$ (Jahr, 1992), led to an estimated K_D of ~224 μM for iMK-801 at −60 mV. The slow on-rate of iMK-801 reflects the reduced access to the binding site that is on the extracellular side of the pore-loop in the NMDAR ion channel (Lu et al., 2017; Song et al., 2018).

Typically, iMK-801 has been used at a concentration of 1 mM, roughly 30,000–200,000 times the dissociation constant of extracellularly applied MK-801 (~5–30 nM; Dravid et al., 2007). The low affinity of iMK-801 to NMDARs can explain why such a high concentration of iMK-801 is required to inhibit NMDAR current. However, such a high concentration of drug may lead to off-target effects on other ion channels or proteins inside the cell. For example, extracellular MK-801 at μM levels can affect acetylcholine receptor signaling (Galligan and North, 1990), and, at mM levels, extracellular MK-801 can affect voltage-gated K^+ channels (Rothman, 1988). Because it is applied through the recording pipette, off-target effects of iMK-801 are difficult to test experimentally.

4.2. Synaptic NMDAR inhibition

In cortical L4-L2/3 synapses, iMK-801 inhibited NMDAR current level to ~25% of the control current level (Fig. 1). In the hippocampal Schaffer collateral-CA1 synapses, inhibition by iMK-801 reduced the

NMDAR current level to ~40–50% of the control current level. These measurements of synaptic NMDAR currents were made while voltage-clamping the neuron to +40 mV in order to relieve Mg^{2+} block of the receptors. Because the interaction of MK-801 with the NMDAR shows voltage dependence, holding at +40 mV may distort the degree of inhibition present at membrane potentials near rest. However, in the reduced HEK-293 cell preparation with recombinant NMDARs, measurements of NMDAR current were possible with no extracellular Mg^{2+} present while holding at −60 mV, near neuronal resting potential, and inhibition by iMK-801 was incomplete.

Another concern with the interpretation of the synaptic experiments is whether iMK-801 inhibition of the NMDAR current has reached a steady-state during the recordings. In the recordings from recombinant receptors holding at −60 mV, inhibition by iMK-801 develops with a time constant of ~5 s in the continued presence of glutamate, while in the synaptic recordings, glutamate is present only briefly after each vesicle release event (Clements et al., 1992). However, even in the case of the recombinant receptors with steady glutamate application, steady-state inhibition of NMDAR currents by iMK-801 was incomplete (Fig. 3). This combination of observations—that the onset of inhibition is slow and that steady-state inhibition is incomplete—underscores the need for caution in interpreting results using iMK-801, and that complete inhibition of NMDAR currents by this manipulation should not be assumed.

4.3. Differences between experimental systems and recording conditions

We found that iMK-801 does not completely inhibit NMDAR current in three different systems: L4-L2/3 synapses in somatosensory cortex from young rats (P14-21), hippocampal Schaffer collateral-CA1 synapses from young mice (P18-24), and recombinant NMDARs expressed in HEK-293 cells. While the qualitative result of incomplete inhibition is shared between each of our experiments, differences between preparations and conditions preclude quantitative comparisons.

The preparations used in this study cover a wide range of glutamate release probabilities. The cortical L4-L23 synapse has a high probability of release (Silver et al., 2003), the hippocampal Schaffer collateral-CA1 synapse has a relatively low probability of release (Dobrunz and Stevens, 1997; Oertner et al., 2002), and, in the case of the recombinant receptors, glutamate was experimentally delivered. Because MK-801 binding requires channel opening (Huettner and Bean, 1988), which in turn requires the presence of glutamate, the time course and steady-state levels of inhibition are likely to be different in the different experimental systems. Manipulating the probability of release in the hippocampal synapses by using a paired-pulse stimulus increased the level of inhibition by iMK-801 (Fig. 2). Although these differences confound direct comparison of the efficacy of iMK-801, in no case was there complete inhibition of NMDAR current.

The recording conditions also varied between the preparations used in this study which confounds direct comparison. For example, the extracellular Mg^{2+} concentration was 1 mM in cortical experiments, 1.3 mM in hippocampal experiments, and 0 mM in recombinant receptor experiments. Higher levels of Mg^{2+} may interfere with MK-801 binding by competing with the MK-801 binding site (McKay et al., 2013). This would be expected to decrease the effectiveness of MK-801 block, exacerbating the incomplete inhibition of NMDAR currents by iMK-801. The extracellular Ca^{2+} concentration also differed between preparations (2 mM in cortical experiments, 2.5 mM in hippocampal experiments, and 0.5 mM in recombinant receptor experiments). Calcium is not known to directly affect MK-801 binding, but it may have indirect effects by altering the rate of NMDAR inactivation (Rosenmund et al., 1995), which would effectively reduce the probability of channel opening and hence MK-801 binding. Similarly, excluding GTP and ATP from the internal solution could increase the rate of rundown of NMDAR current in an experiment which would lead to an overestimation of the effectiveness of iMK-801 to inhibit NMDAR current. Regardless of these differences between experimental conditions, the qualitative result in every case was consistent: the inhibition of the NMDAR current by iMK-801 was incomplete.

Another crucial determinant of NMDAR activity is the subunit identity, which controls receptor kinetics (Cull-Candy and Leszkiewicz, 2004) and could also affect the binding of MK-801. While the synaptic NMDAR subunit composition is not known for certain, it likely contains GluN2A and GluN2B subunits, as either diheteromeric GluN1/GluN2A, GluN1/2B, or triheteromeric GluN1/2A/2B receptors (Monyer et al., 1994; Gray et al., 2011; Tovar et al., 2013). The presence of the GluN2B subunit confers a lower open probability (Erregar et al., 2005; Gray et al., 2011), which would decrease the rate of MK-801 dissociation relative to the rate estimated from the heterologously expressed GluN1/GluN2A receptors (Fig. 3). The uncertainty of the receptor composition in the synaptic systems used in this study hinders quantitative comparisons, but underscores the finding that in no case was inhibition complete.

5. Conclusions

MK-801 has been an extremely useful tool in probing NMDAR channel function, and intracellular MK-801 has been useful in distinguishing NMDAR function in single cells from network effects of NMDAR inhibition. However, we show here 1 mM iMK-801, a commonly used concentration, does not completely inhibit NMDAR currents. This incomplete inhibition can be explained by an extremely slow binding rate of MK-801 when applied to the intracellular side of the membrane. These results are consistent with prior studies that show iMK-801 significantly reduces NMDAR currents, but there is often incomplete block of the current (Humeau et al., 2003; Samson and Pare, 2005; Bender et al., 2006; Corlew et al., 2007; Rodriguez-Moreno et al., 2011; Lavzin et al., 2012; Smith et al., 2013; Larsen et al., 2014). Therefore, while this manipulation can be a useful qualitative tool to selectively reduce NMDAR current in a single recorded cell, it cannot be assumed to eliminate the contribution of NMDAR current to postsynaptic signaling.

Conflicts of interest

The authors declare no conflicts of interest.

Author contributions

WS performed and analyzed the heterologous NMDAR recordings. JMW and JAG performed and analyzed the hippocampal recordings. BCC performed and analyzed the cortical recordings and modeling, and wrote the manuscript. All authors contributed to editing the manuscript.

Acknowledgements

We thank Craig Jahr and Delia Chiu for helpful discussions.
JAG was supported by the Whitehall Foundation.

References

Agmon, A., Connors, B.W., 1991. Thalamocortical responses of mouse somatosensory (barrel) cortex *in vitro*. Neuroscience 41, 365–379.
Beaulieu-Laroche, L., Harnett, M.T., 2018. Dendritic spines prevent synaptic voltage clamp. Neuron 97, 75–82.
Bender, V.A., Bender, K.J., Brasier, D.J., Feldman, D.E., 2006. Two coincidence detectors for spike timing-dependent plasticity in somatosensory cortex. J. Neurosci. 26, 4166–4177.
Berretta, N., Jones, R.S.G., 1996. Tonic facilitation of glutamate release by presynaptic N-methyl-D-aspartate autoreceptors in the entorhinal cortex. Neuroscience 2, 339–344.
Bouvier, G., Bidoret, C., Casado, M., Paoletti, P., 2015. Presynaptic NMDA receptors: roles and rules. Neuroscience 311, 322–340.
Burnashev, N., Zhou, Z., Neher, E., Sakmann, B., 1995. Fractional calcium currents

through recombinant GluR channels of the NMDA, AMPA, and kainate receptor subtypes. J. Physiol. 485, 403–418.
Carter, B.C., Jahr, C.E., 2016. Postsynaptic, not presynaptic NMDA receptors are required for spike-timing-dependent LTD induction. Nat. Neurosci. 19, 1218–1224.
Clements, J.D., Lester, R.A., Tong, G., Jahr, C.E., Westbrook, G.L., 1992. The time course of glutamate in the synaptic cleft. Science 258, 1498–1501.
Corlew, R., Wang, Y., Ghermazien, H., Erisir, A., Philpot, B.D., 2007. Developmental switch in the contribution of presynaptic and postsynaptic NMDA receptors to long-term depression. J. Neurosci. 27, 9835–9845.
Cull-Candy, S.G., Leszkiewicz, D.N., 2004. Role of distinct NMDA receptor subtypes at central synapses. Sci. STKE 255https://doi.org/10.1126/stke.2552004re16. pp. Re16.
Dobrunz, L.E., Stevens, C.F., 1997. Heterogeneity of release probability, facilitation, and depletion at central synapses. Neuron 18, 995–1008.
Dravid, S.M., Erreger, K., Yuan, H., Nicholson, K., Le, P., Lyuboslavsky, P., Almonte, A., Murray, E., Mosley, C., Barber, J., French, A., Balster, R., Murray, T.F., Traynelis, S.F., 2007. Subunit-specific mechanisms and proton sensitivity of NMDA receptor channel block. J. Physiol. 581, 107–128.
Erregar, K., Dravid, S.M., Banke, T.G., Wyllie, D.J., Traynelis, S.F., 2005. Subunit-specific gating controls rat NR1/NR2A and NR1/NR2B NMDA channel kinetics and synaptic signalling profiles. J. Physiol. 563, 345–358.
Galligan, J.J., North, R.A., 1990. MK-801 blocks nicotinic depolarizations of Guinea pig myenteric neurons. Neurosci. Lett. 108, 105–109.
Gray, J.A., Shi, Y., Usui, H., During, M.J., Sakimura, K., Nicoll, R.A., 2011. Distinct modes of AMPA receptor suppression at developing synapses by GluN2A and GluN2B: analysis of single-cell GluN2 subunit deletion in vivo. Neuron 71, 1085–1101.
Hansen, K.B., Ogden, K.K., Yuan, H., Traynelis, S.F., 2014. Distinct functional and pharmacological properties of Triheteromeric GluN1/GluN2A/GluN2B NMDA receptors. Neuron 81, 1084–1096. https://www.ncbi.nlm.nih.gov/pubmed/24607230.
Huettner, J.E., Bean, B.P., 1988. Block of N-methyl-D-aspartate-activated current by the anticonvulsant MK-801: selective binding to open channels. Proc. Natl. Acad. Sci. U.S.A. 85, 1307–1311.
Humeau, Y., Shaban, H., Bissiere, S., Luthi, A., 2003. Presynaptic induction of heterosynaptic associative plasticity in the mammalian brain. Nature 426, 841–845.
Jahr, C.E., 1992. High probability opening of NMDA receptor channels by L-glutamate. Science 255, 470–472.
Jahr, C.E., Stevens, C.F., 1993. Calcium permeability of the N-methyl-D-aspartate receptor channel in hippocampal neurons in culture. Proc. Natl. Acad. Sci. U.S.A. 90, 11573–11577.
Johnson, J.W., Ascher, P., 1987. Glycine potentiates the NMDA response in cultured mouse brain neurons. Nature 325, 529–531.
Kleckner, N.W., Dingledine, R., 1988. Requirement for glycine in activation of NMDA-receptors expressed in Xenopus oocytes. Science 241, 835–837.
Larsen, R.S., Smith, I.T., Miriyala, J., Han, J.E., Corlew, R.J., Smith, S.L., Philpot, B.D., 2014. Synapse-specific control of experience-dependent plasticity by presynaptic NMDA receptors. Neuron 83, 879–893.
Lavzin, M., Rapoport, S., Polsky, A., Garion, L., Schiller, J., 2012. Nonlinear dendritic processing determines angular tuning of barrel cortex neurons in vivo. Nature 490, 397–401.
Lester, R.A., Jahr, C.E., 1992. NMDA channel behavior depends on agonist affinity. J. Neurosci. 12, 635–643.
Lu, W., Du, J., Goehring, A., Gouaux, E., 2017. Cryo-EM structures of the triheteromeric NMDA receptor and its allosteric modulation. Science 355 eaal3729.
Luscher, C., Malenka, R.C., 2012. NMDA receptor-dependent long-term potentiation and long-term depression (LTP/LTD). Cold Spring Harb. Perspect. Biol. 4. https://doi.org/10.1101/cshperspect.a005710.
Lynch, G., Larson, J., Kelso, S., Barrionuevo, G., Schottler, F., 1983. Intracellular injections of EGTA block induction of hippocampal long-term potentiation. Nature 305, 719–721.
Maki, B.A., Popescu, G.K., 2014. Extracellular Ca^{2+} ions reduce NMDA receptor conductance and gating. J. Gen. Physiol. 144, 379–392.
MacDermott, A.B., Mayer, M.L., Westbrook, G.L., Smith, S.J., Barker, J.L., 1986. NMDA-receptor activation increases cytoplasmic calcium concentration in cultured spinal cord neurones. Nature 321, 519–522.
Mayer, M.L., Westbrook, G.L., Guthrie, P.B., 1984. Voltage-dependent block by Mg^{2+} of NMDA responses in spinal cord neurones. Nature 309, 261–263.
McKay, S., Bengtson, C.P., Bading, H., Wyllie, D.J., Hardingham, G.E., 2013. Recovery of NMDA receptor currents from MK-801 blockade is accelerated by Mg^{2+} and memantine under conditions of agonist exposure. Neuropharmacology 74, 119–125.
Monyer, H., Burnashev, N., Laurie, D.J., Sakmann, B., Seeburg, P.H., 1994. Developmental and regional expression in the rat brain and functional properties of four NMDA receptors. Neuron 12, 529–540.
Nevian, T., Sakmann, B., 2006. Spine Ca^{2+} signaling in spike-timing dependent plasticity. J. Neurosci. 26, 11001–11013.
Nowak, L., Bregestovski, P., Ascher, P., Herbet, A., Prochiantz, A., 1984. Magnesium gates glutamate-activated channels in mouse central neurones. Nature 307, 462–465.
Oertner, T.G., Sabatini, B.L., Nimchinsky, E.A., Svoboda, K., 2002. Facilitation at single synapses probed with optical quantal analysis. Nat. Neurosci. 5, 657–664.
Pologruto, T.A., Sabatini, B.L., Svoboda, K. ScanImage, 2003. Flexible software for operating laser scanning microscopes. Biomed. Eng. Online 17 (2), 13.
Rodriguez-Moreno, A., Kohl, M.M., Reeve, J.E., Eaton, T.R., Collins, H.A., Anderson, H.L., Paulsen, O., 2011. Presynaptic induction and expression of timing-dependent long-term depression by compartment-specific photorelease of a use-dependent NMDA receptor antagonist. J. Neurosci. 31, 8564–8569.
Rosenmund, C., Clements, J.D., Westbrook, G.L., 1993. Nonuniform probability of glutamate release at a hippocampal synapse. Science 262, 754–757.
Rosenmund, C., Feltz, A., Westbrook, G.L., 1995. Calcium-dependent inactivation of synaptic NMDA receptors in hippocampal neurons. J. Neurophysiol. 73, 427–430.
Rothman, S., 1988. Noncompetitive N-methyl-D-aspartate antagonists affect multiple ionic currents. J. Pharmacol. Exp. Therapeut. 246, 137–142.
Samson, R.D., Pare, D., 2005. Activity-dependent synaptic plasticity in the central nucleus of the amygdala. J. Neurosci. 25, 1847–1855.
Silver, R.A., Lubke, J., Sakmann, B., Feldmeyer, D., 2003. High-probability uniquantal transmission at excitatory synapses in barrel cortex. Science 302, 1981–1984.
Sjostrom, P.J., Turrigiano, G.G., Nelson, S.B., 2003. Neocortical LTD via coincident activation of presynaptic NMDA and cannabinoid receptors. Neuron 39, 641–654.
Song, X., Jensen, M.Ø., Jogini, V., Stein, R.A., Lee, C.-H., Mchaourab, H.S., Shaw, D.E., Gouaux, E., 2018. Mechanism of NMDA receptor channel block by MK-801 and memantine. Nature 556, 515–519.
Smith, S.L., Smith, I.T., Branco, T., Häusser, M., 2013. Dendritic spikes enhance stimulus selectivity in cortical neurons in vivo. Nature 503, 115–120.
Tovar, K.R., Westbrook, G.L., 2002. Mobile NMDA receptors at hippocampal synapses. Neuron 34, 255–264.
Tovar, K.R., McGinley, M.J., Westbrook, G.L., 2013. Triheteromeric NMDA receptors at hippocampal synapses. J. Neurosci. 33, 9150–9160.
Traynelis, S.F., Wollmuth, L.P., McBain, C.J., Menniti, F.S., Vance, K.M., Ogden, K.K., Hansen, K.B., Yuan, H., Myers, S.J., Dingledine, R., 2010. Glutamate receptor ion channels: structure, regulation, and function. Pharmacol. Rev. 62, 405–496.